

OPEN ACCESS

EDITED BY Hasem Habelhah, The University of Iowa, United States

REVIEWED BY Bruno Tasso, University of Genoa, Italy Emanuela Grassilli, Università Link Campus, Italy

*CORRESPONDENCE
Guido J. R. Zaman

guido.zaman@oncolines.com

RECEIVED 16 July 2025 ACCEPTED 07 October 2025 PUBLISHED 22 October 2025

CITATION

Kluitmans DJF, Melis JJTM, van den Bossche E, Ytsma J, de Roos JADM, van Linden OPJ, Grobben Y, Kooijman JJ and Zaman GJR (2025) Combined cellular and biochemical profiling of Bruton's tyrosine kinase inhibitor nemtabrutinib reveals potential application in MAPK-driven cancers. *Front. Oncol.* 15:1667291. doi: 10.3389/fonc.2025.1667291

COPYRIGHT

© 2025 Kluitmans, Melis, van den Bossche, Ytsma, de Roos, van Linden, Grobben, Kooijman and Zaman. This is an open-access article distributed under the terms of the Creative Commons Attribution License (CC BY). The use, distribution or reproduction in other forums is permitted, provided the original author(s) and the copyright owner(s) are credited and that the original publication in this journal is cited, in accordance with accepted academic practice. No use, distribution or reproduction is permitted which does not comply with these terms.

Combined cellular and biochemical profiling of Bruton's tyrosine kinase inhibitor nemtabrutinib reveals potential application in MAPK-driven cancers

Daphne J. F. Kluitmans¹, Janneke J. T. M. Melis¹, Esmee van den Bossche¹, Jacob Ytsma¹, Jeroen A. D. M. de Roos¹, Oscar P. J. van Linden², Yvonne Grobben¹, Jeffrey J. Kooijman¹ and Guido J. R. Zaman 60 124

¹Oncolines B.V., Oss, Netherlands, ²Division of Innovations in Human Health and Life Sciences, Amsterdam Institute of Molecular and Life Sciences, Faculty of Science, Vrije Universiteit Amsterdam, Amsterdam, Netherlands

Background: Nemtabrutinib is a reversible inhibitor of both wild-type and acquired resistance-related mutant BTK. Since nemtabrutinib biochemically inhibits various kinases, new drug response biomarkers, cross-reactivities and differentiators may be identified.

Methods: Nemtabrutinib was profiled in a large panel of cancer cell line viability assays. The sensitivity profile of nemtabrutinib was compared with the profiles of 135 kinase inhibitors across the same cell lines. Additionally, cell line sensitivity was related to gene mutation status, gene and protein expression levels, and gene dependency scores. Potential targets were explored using biochemical assays.

Results: Sensitivity to nemtabrutinib is on average three times higher in *BRAF*-mutant *versus* wild-type cell lines. Consistently, the sensitivity profile of nemtabrutinib is similar to that of MEK, ERK and pan-RAF inhibitors. Furthermore, sensitivity to nemtabrutinib is correlated with high *FGFR3* gene expression levels, high levels of phosphorylated MEK1 and genetic dependency on several mitogenactivated protein kinases (MAPK). Biochemical profiling confirms that nemtabrutinib inhibits several growth factor receptor tyrosine kinases and downregulates MAPK signaling via MEK. Molecular docking studies suggest that nemtabrutinib preferentially binds in the ATP-binding pocket of MEK1.

Conclusion: Combined cancer cell panel and biochemical profiling reveals previously underappreciated cross-reactivities of nemtabrutinib indicating a potential application in MAPK-driven cancers.

KEYWORDS

cancer cell line proliferation, Bruton's tyrosine kinase (BTK), bioinformatics, kinase profiling, MAPK, Biacore, kinase inhibitor

1 Background

Cancer cell panel profiling is the parallel testing of drugs on large panels of human cancer cell lines in cell viability assays (1). Predictive biomarkers of drug response can be identified by relating drug sensitivity to genomic information of the cell lines (2–7). In addition, comparing the sensitivity profile of different drugs profiled on the same cell line panel can help in elucidating their biochemical mechanisms of action (8). For example, the profile of the Bruton's tyrosine kinase (BTK) inhibitor ibrutinib in the Oncolines[®] cancer cell line panel shows similarity with that of epidermal growth factor receptor (EGFR) tyrosine kinase inhibitors (5). This is in accordance with the biochemical inhibition of EGFR by ibrutinib (9), which has been related to its major clinical adverse effects (diarrhea and rash) (10).

BTK plays a key role in oncogenic B-cell signaling and is a molecular target for the development of therapies against various Bcell malignancies. Currently, four small-molecule BTK inhibitors have been approved by the U.S. Food and Drug Administration (FDA) for treatment of mantle cell lymphoma, chronic lymphocytic leukemia and small lymphocytic lymphoma. The first three approved drugs (i.e., ibrutinib, acalabrutinib and zanubrutinib) are covalent inhibitors that bind irreversibly to a cysteine residue (C481) in the active site of BTK. In more than 50% of patients treated with these inhibitors, clinical drug resistance is associated with amino acid substitutions at position C481 in BTK (11-13). These substitutions, which mostly involve conversion to serine, but also to arginine, preclude the binding of covalent inhibitors (11–13). To overcome this mechanism of acquired resistance, the reversible inhibitors pirtobrutinib (LOXO-305) (14) and nemtabrutinib (MK-1026; ARQ 531) (15) targeting both wild-type and C481-mutant BTK were developed. Pirtobrutinib received market authorization in 2023, while nemtabrutinib is still under investigation in phase 3 clinical trials for B-cell malignancies (16).

In this study, cell panel profiling experiments and bioinformatic analyses were performed for nemtabrutinib to identify predictive drug response biomarkers and differentiators towards approved BTK inhibitors. Several kinases not previously described to be involved in the cellular response of nemtabrutinib, including various mitogen-activated protein kinases (MAPKs), were identified as potential predictive drug response markers. Biochemical kinase assays confirmed that some of these kinases are a direct molecular target of nemtabrutinib.

2 Methods

2.1 BTK inhibitors

Nemtabrutinib and pirtobrutinib were purchased from ChemScene LLC (Monmouth Junction, NJ, USA). Acalabrutinib, ibrutinib and zanubrutinib were purchased from MedChemExpress LLC (Monmouth Junction, NJ, USA), Axon Medchem B.V. (Groningen, the Netherlands), and Activate Scientific GmbH (Prien am Chiemsee, Germany), respectively. All inhibitors were

stored as dry powders at 4 °C and were dissolved in dimethyl sulfoxide (DMSO) at 10 mmol/L concentration before testing.

2.2 Kinase assays

Nemtabrutinib and the approved BTK inhibitors were profiled on a panel of 254 wild-type kinases in mobility shift assays (MSA) at Carna Biosciences, Inc. (Kobe, Japan). Kinase inhibition was measured at a compound concentration of 1 µmol/L and an ATP concentration of $K_{\text{M,bin}}$ (17), which is an ATP concentration within 2-fold of the affinity of an individual kinase for ATP ($K_{M,ATP}$). Percentage inhibition values were mapped to a phylogenetic kinome tree using Coral (http:// phanstiel-lab.med.unc.edu/CORAL/, accessed September 4th, 2024) (18). Half-maximal inhibitory concentration (IC₅₀) values were determined using duplicate 10-point dilution series in MSA at Carna Biosciences, Inc. for 15 kinases, while for MEK1 and MEK2, inhibition of enzymatic activity was measured in-house in enzyme-linked immunosorbent assays (ELISA) (Carna Biosciences, Inc., cat. no. 07-41 and 07-42). Percentage inhibition of MEK1 and MEK2 at 1 μ mol/L nemtabrutinib and $K_{M,bin}$ ATP concentration was derived from the dose-response curve as well and mapped to the phylogenetic kinome tree, as described above. Inhibition of MLK1 and B-RAF at $K_{M,ATP}$ was determined in a radiometric assay using 32P-labeled ATP at Eurofins Cerep SA (Celle-Lévescault, France). Interaction with SIK3 was assessed in a competition binding assay at Eurofins DiscoverX LLC (San Diego, CA, USA). The binding of nemtabrutinib to biotinylated, inactive MEK1 (Carna Biosciences, Inc., cat. no. 07-441-10-20N) and activated B-RAF (Carna Biosciences, Inc., cat. no. 09-422-20N) was measured by surface plasmon resonance (SPR) using a Biacore 1S+ (Cytiva), as described previously (9).

2.3 Cell line panel

A panel of 160 cancer cell lines was used in this study. Supplementary Table S1 provides an overview of the 160 cell lines used for cell viability assays, the subset of 102 cell lines used for comparative profiling and the subsets used for different bioinformatic analyses, which were dependent on the availability of public data. Cell lines were purchased from the American Type Culture Collection (ATCC) (Manassas, VA, USA), the German Collection of Microorganisms and Cell Cultures (DSMZ) (Braunschweig, Germany), the RIKEN BioResource Research Center (Tsukuba, Ibaraki, Japan) or the Japanese Collection of Research Bioresources (JCRB) (Ibaraki City, Osaka, Japan). All cell lines were propagated in the cell culture media as indicated in Supplementary Table S1. Cell viability assays were carried out within ten passages of the original vials. The authenticity of the ATCC and DSMZ cell lines has been confirmed by short tandem repeat analysis at both institutions. In addition, the mutation status of several cancer genes has been confirmed in various cell lines, including RIKEN and JCRB cell lines, by next-generation sequencing of genomic DNA isolated from the same cell batches as used for the viability assays (19, 20).

2.4 Cell viability assays

Intracellular ATP content was used as an indirect readout of cell number using the ATPlite 1Step bioluminescence assay (Revvity, Groningen, the Netherlands). Cells were seeded in 384-well plates at an optimized density to ensure unrestricted growth and maximal signal at the end of the experiment. After 24 hours of incubation, the starting cell number was determined by adding ATPlite to each well of a control plate and recording luminescence on an Envision multimode reader (Revvity, Waltham, MA, USA) (4). Compounds were diluted in DMSO in √10-fold steps from 10 mmol/L stocks to obtain 9-point dilution series. After further 31.6-fold dilution in 20 mmol/L HEPES (pH 7.4), the dilution series were added in duplicate to the cells in the 384-well plates to determine the effect of the compounds on cell viability. Vehicle-treated controls were included to determine maximal cell proliferation. The final DMSO concentration was 0.4% (v/v) in all wells. After incubation for an additional 72 hours, the ATP content was measured in each well using ATPlite. The luminescent signal in inhibitor-treated wells was normalized to vehicle-treated control wells to determine the percentage viability at each concentration. Cell doublings were determined by relating the cell number of vehicletreated controls to the starting cell number for each cell line. The viability assay of a cell line was repeated when the cell doubling deviated > 2-fold from the historic doubling as determined by multiple independent experiments. The quality of the complete assay was determined by a parallel test with doxorubicin on two cell lines. IC₅₀ values were calculated by fitting a four-parameter logistic model to the percentage viability values using IDBS XLfit5 (IDBS, Guildford, United Kingdom). All curves were visually inspected and submitted to an F-test as implemented in IDBS XLfit5. Curves with an F-value above 1.5 were invalidated and IC50 values were maximized at the highest concentration. The highest initial test concentration in each dose range was 31.6 µmol/L and the lowest was 3.16 nmol/L. When this dose range was too high in a certain cell line to allow for a reliable determination of the IC₅₀, a new dilution series was prepared using a diluted stock solution and was used to retest the compound on the cell line.

2.5 Datasets

Multiple datasets were used for the bioinformatic analyses. The gene mutation, fusion and amplification status of the cell lines were retrieved from the COSMIC Cell Lines Project available at the COSMIC database (https://cancer.sanger.ac.uk) (21), the DepMap database (release 24Q2) (7) and literature. Mutations were filtered for oncogenic relevance with the Cancer Hotspots database (https://www.cancerhotspots.org/#/home) (22) and the OncoKB database (https://www.oncokb.org/) (23, 24), as described previously (6). Gene mutation data are available for 156 of the 160 profiled cell lines (Supplementary Table S1).

The in-house Oncolines[®] kinase inhibitor dataset contains the IC_{50} profiles of 135 kinase inhibitors that have been profiled on a subset of 66 or 102 of the 160 cancer cell lines. The kinase inhibitor set includes approved drugs, clinical and pre-clinical inhibitors, and tool compounds (Supplementary Table S2).

Gene and protein expression data of cell lines as well as gene dependency scores were retrieved from the DepMap database (7). Basal mRNA gene expression levels (release 23Q4) were used and are available for 145 of the 160 profiled cell lines (Supplementary Table S1). Protein expression levels, as determined by Reverse Phase Protein Array (release 22Q2), were used and are available for 128 of the 160 cancer cell lines (Supplementary Table S1).

Gene dependency scores from a large individual CRISPR knock-out screen and large RNA interference (RNAi) knockdown screens (release 23Q4 and Demeter Data v6, respectively) were used (25–29). In these screens, the effect of single-gene knockout or knock-down on cell viability has been determined. The more negative a dependency score, the more dependent a cell line is on a specific gene. The CRISPR dataset includes data for 120 of the 160 profiled cell lines, while the RNAi dataset covers data for 107 of the 160 cell lines (Supplementary Table S1).

2.6 Bioinformatics

For all bioinformatic analyses of cell viability assay data, $^{10}logIC_{50}$ values (in nmol/L) were used as a measure for cell line sensitivity. All calculations were performed in R (version 4.3.1) (30).

For the gene mutation analysis, profiled cell lines were classified as having an alteration in a gene if the gene was mutated, fused, amplified (oncogenes) or deleted (tumor suppressor genes). Otherwise, cell lines were classified as 'wild-type'. The analysis focused on a subset including known oncogenic kinase genes (31) of which only 23 genes that were altered in three or more cell lines were included to allow for proper statistics. A type II analysis of variance (ANOVA) was performed to identify significant associations between cell line sensitivity to nemtabrutinib and kinase gene alterations. Significance after multiple testing correction was determined with the Benjamini-Hochberg procedure (*i.e.*, false discovery rate < 20%).

The IC_{50} profile of nemtabrutinib was compared to the IC_{50} profiles of the kinase inhibitors in the Oncolines kinase inhibitor dataset by calculating the Pearson correlation between compounds or by hierarchical clustering. The network tree of inhibitors and Pearson correlations was generated using the Fruchterman–Reingold algorithm, as implemented in the R package igraph (32). Hierarchical clustering of cell panel viability data from the kinase inhibitors was performed with the Ward method, using 1 – Pearson correlation (r) as clustering distance, as described previously (8).

The IC $_{50}$ values of nemtabrutinib were correlated to basal gene expression levels of 371 genes and protein expression levels of 55 genes that have been experimentally determined to be involved in cancer (33) using Pearson correlations. Additionally, Pearson correlations were determined between the IC $_{50}$ values of nemtabrutinib and CRISPR or RNAi dependency scores of 465 and 204 kinase genes, respectively (34). Significance of all correlations was determined by calculating p-values, which were subjected to the Benjamini-Hochberg procedure to correct for multiple testing. Correlations with a false discovery rate of < 20% were considered significant.

2.7 Computational modeling

Docking of nemtabrutinib in the ATP- and allosteric binding pocket of MEK1 was performed with the structure of MEK1 with the ATP-competitive MEK1 inhibitor DS03090629 (PDB ID:7XLP (35)) and the structure of MEK1 with adenosine 5'-(β , γ -methylene) triphosphate (AMP-PCP) and allosteric MEK1 inhibitor cobimetinib (PDB ID: 4AN2 (36)), respectively. Prior to docking, the structures were processed in MOE v2024.06, hydrogen atoms were added, partial charges were calculated using the Amber10: EHT forcefield and energy minimization was performed. The ATP-and allosteric binding pockets were selected as amino acids within 4.5 Å distance of DS03090629 and cobimetinib, respectively. DS03090629, cobimetinib and co-factors not involved in ligand binding were removed from the structures. Docking in the allosteric binding pocket was done in the presence of AMP-PCP and magnesium.

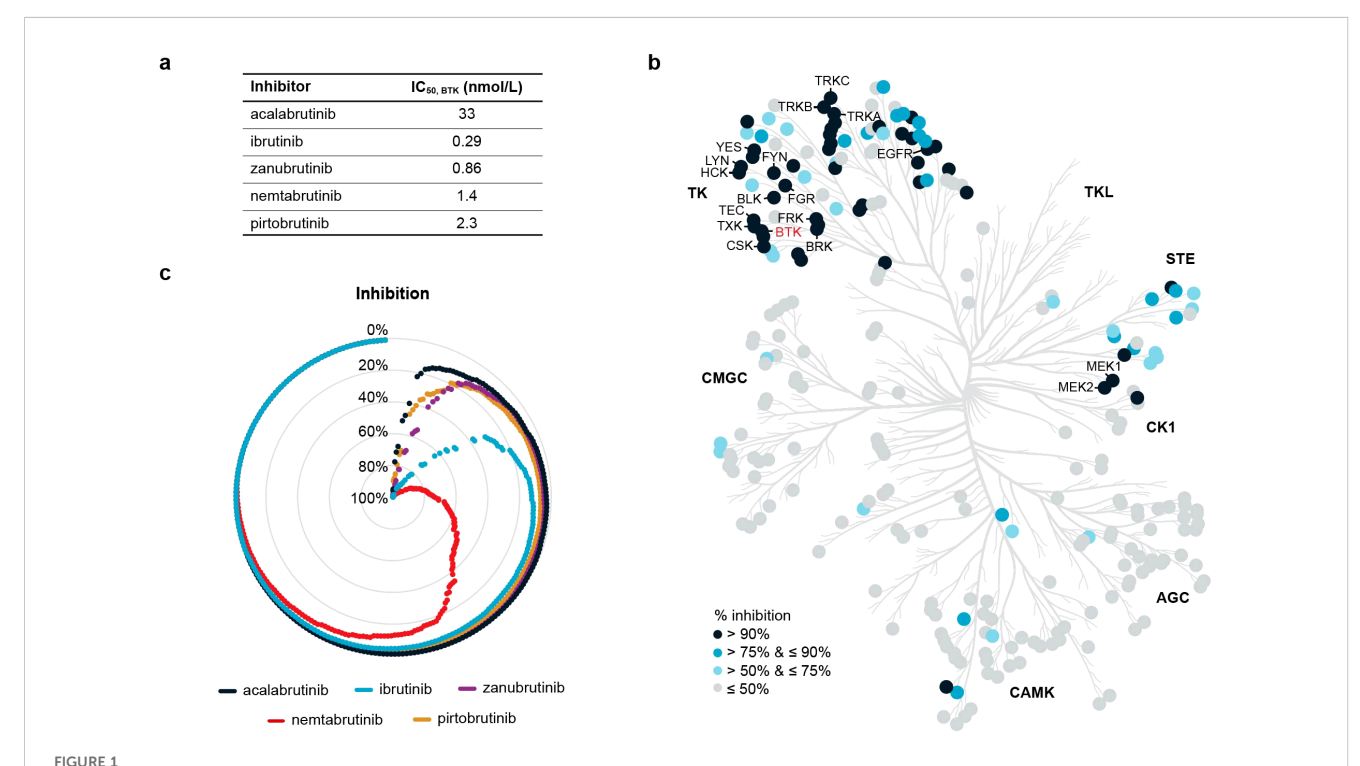
Docking was performed using the Amber10:EHT forcefield with Triangle Matcher placement and Induced Fit receptor refinement. Redocking of DS03090629 and cobimetinib in their respective protein structures validated the docking procedure (RMSDs: 0.61 and 0.92; docking scores: -12.2 and -10.1). Docking scores for nemtabrutinib in the ATP-binding pocket ranged from -10.9 to -10.5. For docking of nemtabrutinib in the allosteric binding pocket, 100 docking poses were generated of which the 25 highest-scoring poses after refinement (-9.8 to -8.9) were

reported. Docking poses were visually inspected and analyzed for ligand-protein interactions using interaction fingerprints (IFPs).

3 Results

3.1 Kinome profiling

Nemtabrutinib inhibited the tyrosine kinase activity of wildtype BTK in biochemical assays with an IC₅₀ of 1.4 nmol/L, which is in range with the inhibition of BTK by the approved BTK inhibitors (Figure 1a). The acquired resistance-related C481S-mutant BTK is inhibited by nemtabrutinib with a similar IC_{50} (1.6 nmol/L, Table 1). As previously noted (15), nemtabrutinib shows crossreactivity with many other kinases in biochemical assays, including other TEC family, SRC family and growth factor receptor tyrosine kinases (RTKs) (Figure 1b, Table 1). When profiled on a panel of 254 wild-type kinases at a single concentration of 1 μmol/L, nemtabrutinib inhibited the activity of 63 kinases by more than 75% and 45 kinases by more than 90% (Figure 1b, Supplementary Table S3). This is a considerably higher number of cross-reactivities than found for the approved BTK inhibitors on the same kinase panel (Figure 1c, Supplementary Table S3). For example, the other reversible BTK inhibitor pirtobrutinib inhibited only five kinases by more than 75% (i.e., Aurora B, BRK, CSK, EGFR and TEC) (Supplementary Table S3). These results indicate that



Biochemical kinase profiling. (a) Biochemical IC₅₀ values of nemtabrutinib and four approved BTK inhibitors on BTK. (b) Phylogenetic tree of human protein kinases highlighting 256 wild-type kinases that were examined for inhibition by nemtabrutinib in profiling experiments. Enzyme assays were performed at $K_{M,bin}$ ATP and 1 µmol/L nemtabrutinib. (c) Radar chart of the percentage inhibition of 254 wild-type kinases in the presence of 1 µmol/L nemtabrutinib or one of the four approved BTK inhibitors. Each dot represents a kinase and the kinases are ordered based on percentage inhibition per inhibitor.

TABLE 1 $\,$ IC₅₀ of nemtabrutinib in kinase enzyme activity assays performed at $K_{\rm M.bin}$ ATP or 1 mmol/L ATP.

Kinase		IC ₅₀ in nmol/L	
Gene	Protein	K _{M,bin} ATP	1 mmol/L ATP
BRAF	B-RAF	73.0 ¹	335
BRAF [V600E]	B-RAF [V600E]		220
BTK	BTK	1.42	
BTK [C481S]	BTK [C481S]	1.60	
FGFR1	FGFR1	134	
FGFR2	FGFR2	34.0	
FGFR3	FGFR3	70.1	
FGFR4	FGFR4	1,400	
MAP2K1	MEK1	8.46	456
MAP2K2	MEK2	9.50	494
MAP3K9	MLK1 ¹	4,870	
MAPK3	ERK1	543	
MAPK1	ERK2	505	
PDGFRA	PDGFRα	12.4	
SIK3	SIK3	> 10,000 ^{1,2}	9,320
TEC	TEC	0.750	
YES	YES	0.591	

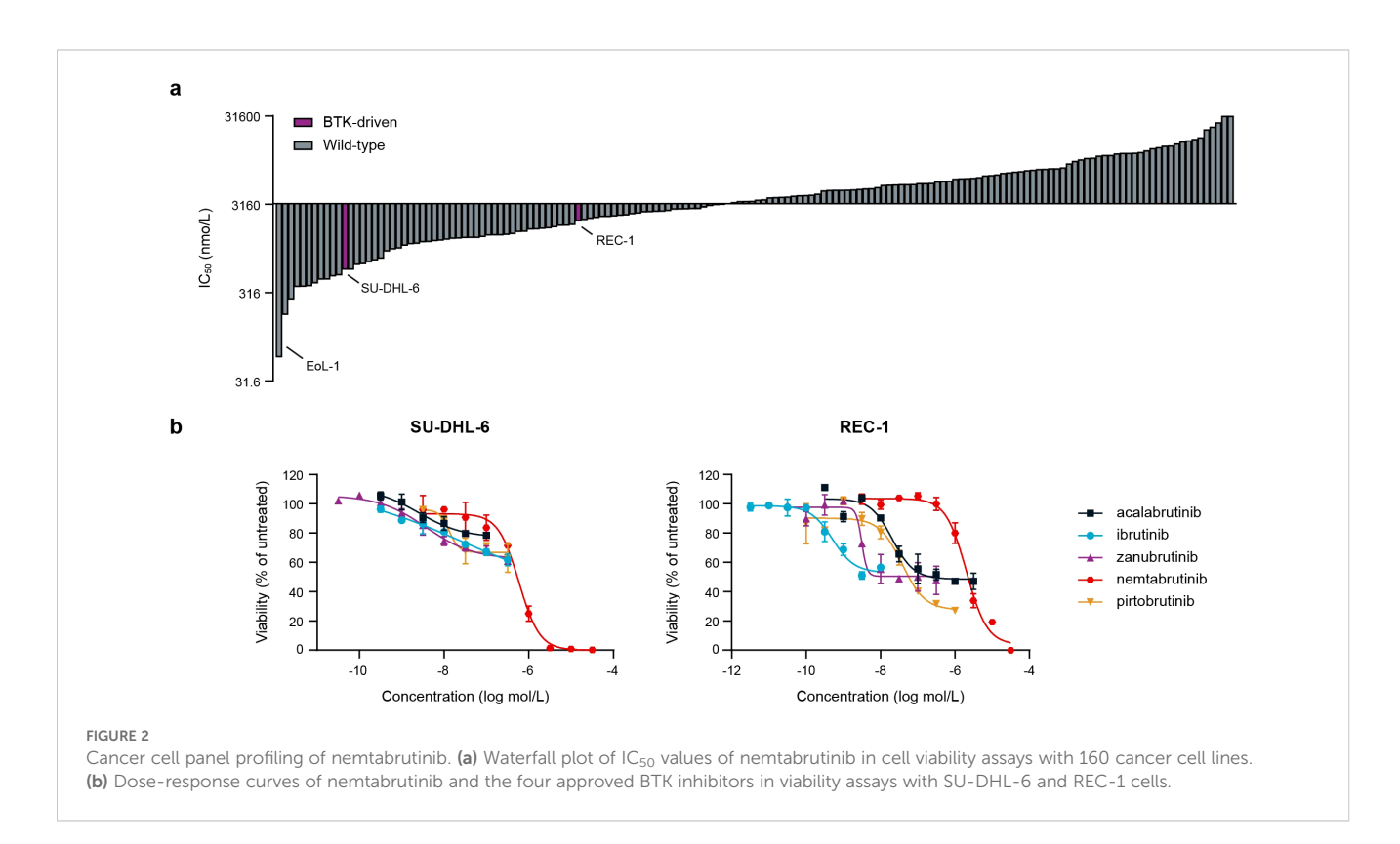
¹Assays performed at Eurofins. All other assays were performed at Carna biosciences, Inc. or in-house

nemtabrutinib has a broader selectivity in biochemical assays compared to pirtobrutinib and the approved irreversible BTK inhibitors.

3.2 Cancer cell line profiling

To study the activity and selectivity of nemtabrutinib in cancer cells, nemtabrutinib was profiled on a panel of 160 human cancer cell lines in cell viability assays. The cell panel represents a wide range of solid tumors and hematological malignancies (Supplementary Table S1). Nemtabrutinib demonstrated potent inhibitory activity across cell lines from all tissues and disease types. The most sensitive cell line was the chronic eosinophilic leukemia cell line EoL-1 (IC₅₀ = 59 nmol/L), expressing a fusion gene of Factor Interacting with PAPOLA and CPSF1 (FIP1L1) and platelet-derived growth factor receptor α (PDGFRα) (Figure 2a, Supplementary Table S4) (37). Other cell lines among the most sensitive responders were two T-cell acute lymphoblastic leukemia (T-ALL) cell lines (Jurkat E6.1 and CCRF-HSB-2) and several cell lines derived from solid tumors, including endometrial (HEC-251 and HEC-1-B) and colon cancers (HT-29). The germinal center Bcell like diffuse large B-cell lymphoma (DLBCL) cell line HT and the prostate carcinoma cell line LNCaP clone FGC were among the least sensitive cell lines in the viability assays (IC₅₀ > 31.6 μ mol/L) (Supplementary Table S4).

The profiled cancer cell line panel contains two cell lines derived from BTK-dependent cancers, *i.e.*, the DLBCL cell line SU-DHL-6 and the mantle cell lymphoma cell line REC-1. The SU-DHL-6 cell line harbors a mutation in *MYD88* resulting in the activation of BTK



in-nouse.

Assay was a ligand competition assay instead of an enzyme activity assay.

(38), while the REC-1 cell line has constitutively active B-cell receptor signaling (39). Nemtabrutinib inhibited the viability of these cell lines with an IC $_{50}$ of 0.6 μ mol/L and 2.0 μ mol/L, respectively. This contrasts the potent IC $_{50}$ values of the irreversible BTK inhibitors ibrutinib, acalabrutinib and zanubrutinib on these cell lines (Figure 2b, Supplementary Table S5). However, the approved BTK inhibitors showed only partial effects, while nemtabrutinib reached almost complete inhibition of viability (Figure 2b).

3.3 Bioinformatic analysis of cell panel profiling data

To investigate which kinases could be responsible for the broad cellular activity of nemtabrutinib, a number of bioinformatic analyses were performed on the cell panel profiling data. Both genomic alterations and aberrant expression of genes or proteins can induce tumor cell proliferation (31, 33). Therefore, we correlated the IC_{50} profile of nemtabrutinib with the mutation status of oncogenic kinases, the gene dependency scores of human kinase genes and with the gene or protein expression levels of known cancer genes in the cell lines.

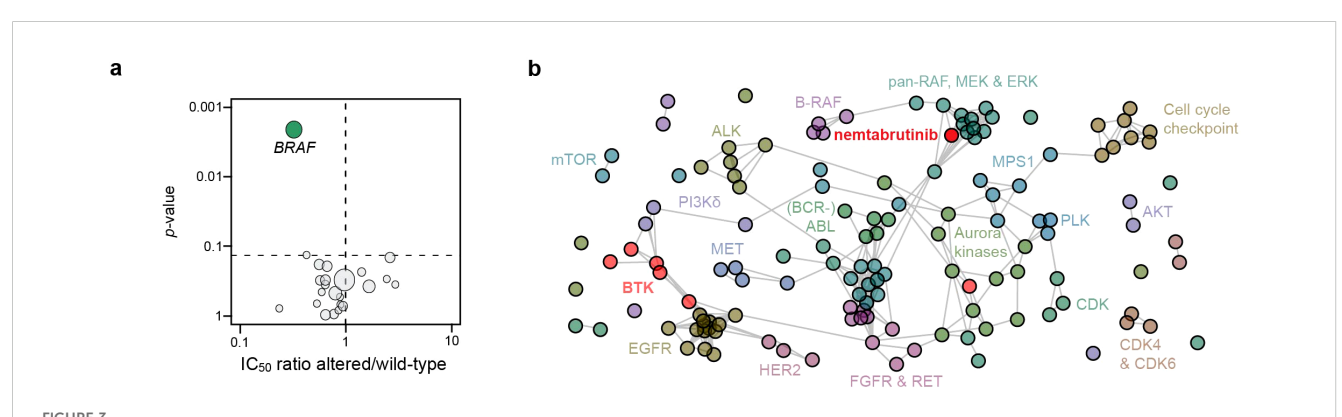
Associations between cell line sensitivity and gene mutations were determined by ANOVA. Of the 23 kinase genes analyzed, only the mutation status of *BRAF* was found to be significantly associated with nemtabrutinib sensitivity (Figure 3a). Cancer cell lines harboring mutations in *BRAF* were on average three times more sensitive than cell lines expressing wild-type *BRAF*. Mutant *BRAF* is also a predictive biomarker of drug response for B-RAF and MEK1 inhibitors profiled in our cancer cell line panel (4, 6).

To further investigate the mechanism underlying the association of cell line sensitivity to nemtabrutinib with BRAF mutation status, we compared the IC_{50} profile of nemtabrutinib with the profiles of the 135 kinase inhibitors in the Oncolines kinase inhibitor dataset in a one-to-one comparison analysis. Inhibitors are considered to have a similar inhibitory profile if the Pearson correlation is 0.5 or higher. If inhibitors show a similar

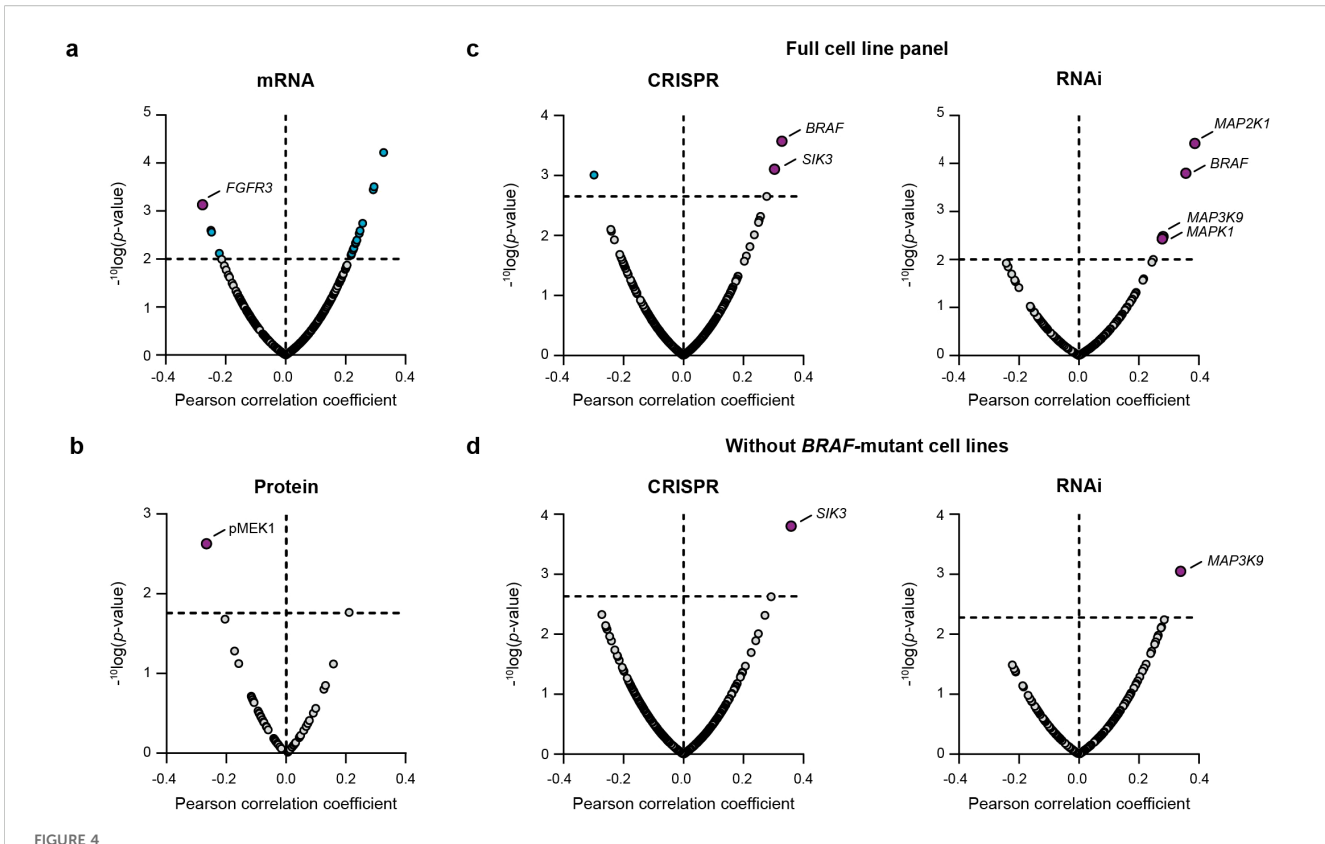
profile, they are connected to each other in a network tree for visualization (Figure 3b). The analysis revealed that nemtabrutinib is not connected with the approved BTK inhibitors, but shows connections with MEK, ERK and pan-RAF inhibitors (Figure 3b). A comparative analysis based on an unsupervised hierarchical clustering showed similar results (Supplementary Figure S1). The approved BTK inhibitors cluster at distant locations in the hierarchical clustering tree. For instance, and as noted before (8), ibrutinib clusters with EGFR inhibitors (Supplementary Figure S1).

Basal gene expression levels of 371 cancer genes were correlated to the cancer cell line sensitivity of nemtabrutinib. This correlation analysis revealed increased expression of fibroblast growth factor receptor 3 (*FGFR3*) as a significant marker of drug response (Figure 4a). Cancer cell line sensitivity was also correlated to the protein expression levels of 55 cancer genes. This showed that high levels of phosphorylated MEK1 are significantly correlated with sensitivity to nemtabrutinib (Figure 4b).

Finally, we compared the drug sensitivity profile of nemtabrutinib with the genetic dependency scores of kinase genes available from large-scale CRISPR (465 genes) and RNAi screens (204 genes). Significant positive correlations were found between the IC50 profile of nemtabrutinib and the CRISPR knock-out dependency scores of two genes: BRAF and SIK3 (Figure 4c). Knock-down of BRAF by RNAi was also significantly correlated with response to nemtabrutinib. Additionally, response to nemtabrutinib exhibits a strong positive correlation with knockdown dependency scores of MAP2K1, MAP3K9, and MAPK1 (Figure 4c), encoding the MAPK pathway components MEK1, MLK1 and ERK2. The correlation analysis was repeated with the dataset minus the 16 BRAF-mutant cell lines to determine whether the preferential targeting of BRAF-mutant cell lines by nemtabrutinib may have strongly influenced the results. The significant positive correlations with SIK3 and MAP3K9 in the CRISPR and RNAi screen dataset, respectively, were maintained in this analysis (Figure 4d), indicating that the dependency of cell lines on these kinases can predict nemtabrutinib response independent of BRAF mutation status.



Cancer gene mutation analysis and comparative profiling. (a) Volcano plot showing the correlation of nemtabrutinib response in cell viability assays with the mutation status of 23 oncogenic kinases in the cell lines. Each circle represents a kinase gene that is mutated in at least three cell lines. (b) Network tree connecting inhibitors with a similar profile. In case the Pearson correlation coefficient of the IC_{50} fingerprint of two compounds is 0.5 or higher, a connection is drawn in the network. The length of the line has no meaning. Nemtabrutinib and the BTK inhibitors are colored in red.



Bioinformatic correlation analyses of cancer cell line sensitivity to nemtabrutinib. (a) Volcano plot of Pearson correlation coefficients of IC_{50} values in cell viability assays and basal expression levels of 371 cancer genes. (b) Volcano plot of Pearson correlation coefficients of IC_{50} values in cell viability assays and expression levels of 55 cancer proteins. (c) Volcano plot of Pearson correlation coefficients of response profiles and gene dependency scores from gene knock-out (CRISPR) or knock-down (RNAi) screens. (d) Results from same analysis as in panel c, after exclusion of the 16 BRAF-mutant cell lines.

3.4 Kinase biochemical inhibition

To determine whether the kinases identified in the bioinformatic analyses of the cell panel profiling study were genuine biochemical targets of nemtabrutinib, kinase enzyme activity assays were performed. The IC₅₀ values of nemtabrutinib in biochemical assays with these kinases are given in Table 1. Table 1 summarizes a subset of kinases that were included in the panel of 254 wild-type kinases for the single concentration profiling (Supplementary Table S3), such as FGFR1-4, as well as kinases that were not included in this panel (MEK1, MLK1, ERK2, B-RAF and SIK3).

The most sensitive cell line EoL-1 has a constitutively active PDGFR α due to a FIP1L1-PDGFR α fusion (37). In a biochemical assay, PDGFR α was inhibited with an IC₅₀ of 12.4 nmol/L. As mentioned before, the gene expression analysis revealed a correlation between high expression of *FGFR3* and cell line sensitivity to nemtabrutinib (Figure 4a). Biochemically, nemtabrutinib inhibits FGFR3 with an IC₅₀ of 70.1 nmol/L and FGFR2 is even more potently inhibited with an IC₅₀ of 34.0 nmol/L. For FGFR1, moderately potent inhibition was found (IC₅₀ = 134 nmol/L), while FGFR4 was not potently inhibited (IC₅₀ = 1.40 μ mol/L). The cell lines AN3-CA and KATO III have an *FGFR2* mutation or amplification, respectively (6). These cell lines were

inhibited by nemtabrutinib with a potency within the range of inhibition of the BTK-driven cell lines (IC₅₀ = 1.1 μ mol/L) (Supplementary Table S4). The *FGFR1* fusion-positive cell line KG-1 and *FGFR3* fusion-positive cell line RT-4 (6) are also inhibited within that range, however with a slightly lower potency (IC₅₀ = 1.4 and 1.7 μ mol/L, respectively). No binding to SIK3 by nemtabrutinib was found (Table 1). These results suggest that platelet-derived and fibroblast growth factor receptors are potential drug response biomarkers for nemtabrutinib.

The sensitivity of BRAF-mutant cell lines to nemtabrutinib indicates activity of nemtabrutinib on the MAPK pathway. Nemtabrutinib inhibited MEK1 and MEK2 with IC50 values of 8.5 and 9.5 nmol/L, respectively (Table 1). The compound also showed inhibitory activity in the B-RAF assay with an IC50 of 73 nmol/L. It should be noted that the B-RAF kinase assay is a cascade assay, in which activity is indirectly measured via MEK1 and ERK2. Nemtabrutinib did not inhibit MLK1, ERK1 or ERK2 (Table 1).

3.5 Kinase binding and computational modeling

To investigate the specific target of nemtabrutinib in the MAPK pathway, surface plasmon resonance binding experiments were

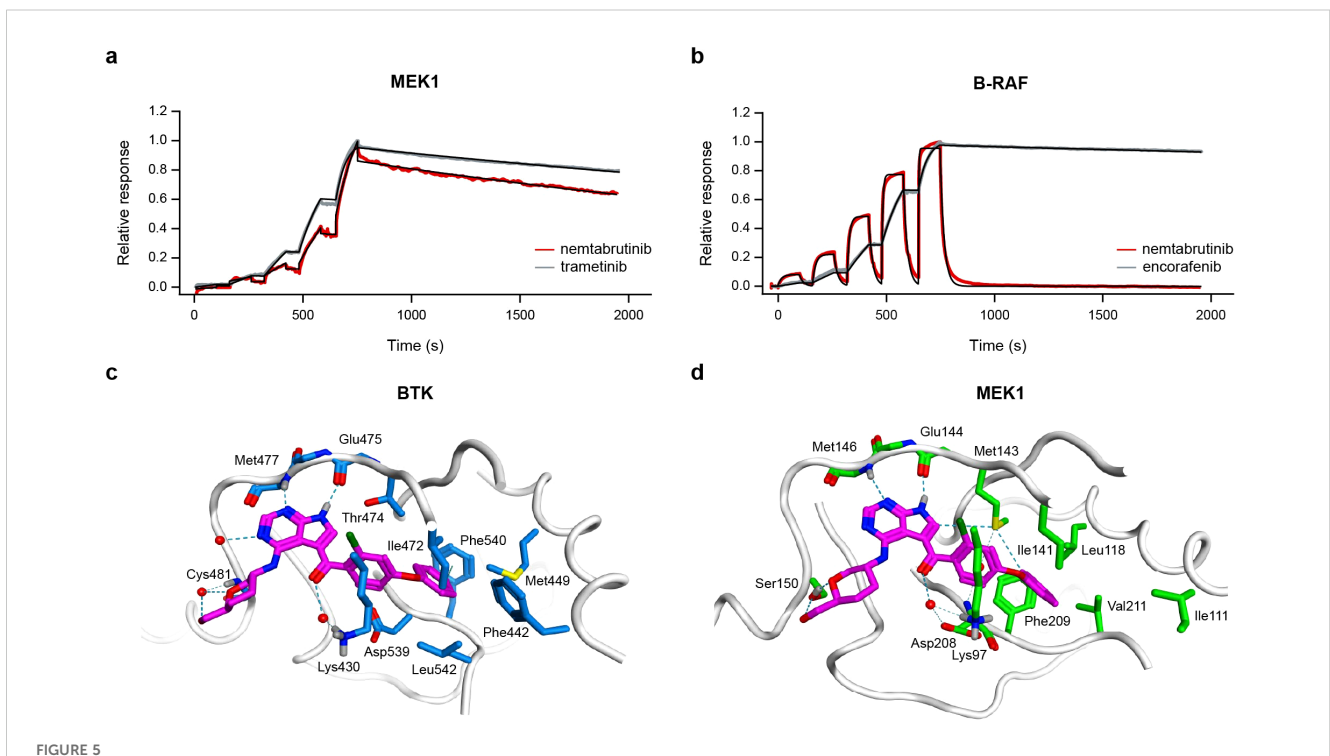
performed on B-RAF and MEK1. Nemtabrutinib bound inactive MEK1 with an affinity ($K_{\rm D}$) of 10 nmol/L (Figure 5a), whereas it bound activated B-RAF with a $K_{\rm D}$ of 1.2 µmol/L (Figure 5b), corresponding to a 120-fold difference in affinity (Supplementary Table S6). This indicates that the inhibitory effect on MAPK signaling is most likely due to inhibition of MEK1 rather than B-RAF.

X-ray crystallographic studies on nemtabrutinib-bound BTK indicate that nemtabrutinib is an ATP-competitive BTK inhibitor (Figure 5c, Supplementary Table S7) (15). To investigate the binding mode of nemtabrutinib in MEK1, molecular docking in both the ATP- and allosteric binding pocket of MEK1 was performed. Docking of nemtabrutinib in the ATP-binding pocket of MEK1 resulted in multiple docking poses, which were described by interaction fingerprints (IFPs). These in silico predicted IFPs were compared to the IFP derived from the X-ray crystallographic analysis of the nemtabrutinib-BTK complex (15). Interestingly, the highest-scoring docking pose of nemtabrutinib in MEK1 has a very similar IFP as the IFP found in the crystal structure of nemtabrutinib-bound BTK (Figures 5c, d, Supplementary Table S7). This includes two hydrogen bond interactions between the pyrrolo-pyrimidine ring of nemtabrutinib and two hinge region residues in the ATP-binding pocket of BTK (Met⁴⁷⁷ and Glu⁴⁷⁵) and MEK1 (Met146 and Glu144). Additionally, the hydroxymethyloxane moiety and the carbonyl oxygen atom of nemtabrutinib forms a (water-mediated) hydrogen bond interaction with the residues Cys⁴⁸¹ and Lys⁴³⁰ (BTK) or Ser¹⁵⁰ and Lys⁹⁷ (MEK1), respectively.

In contrast, docking of nemtabrutinib in the allosteric pocket of MEK1 indicates that nemtabrutinib exhibits extensive sampling of the allosteric pocket, suggesting a lack of strong and highly complementary interactions. Oppositely, the crystal structure of cobimetinib in the allosteric pocket of MEK1 showed multiple polar contacts, such as hydrogen bond interactions with Lys⁹⁷, Asp¹⁹⁰ and Met¹⁴³ as well as halogen bond interactions with Val¹²⁷ and Ser²¹² (Supplementary Figure S2A). Indeed, the IFP analysis shows that nemtabrutinib is unable to form the contacts observed with cobimetinib (Supplementary Figure S2B, C). Altogether, the molecular docking experiments suggest that nemtabrutinib preferentially binds to the ATP-binding pocket and does not exhibit strong binding to the allosteric pocket.

4 Discussion

Both mutations in kinase genes and their increased expression can cause aberrant tumor growth. To identify the kinases responsible for the anti-proliferative activity of nemtabrutinib in cell lines, we determined associations between cancer cell line sensitivity and gene mutation status. Additionally, we compared the IC_{50} profile of nemtabrutinib with the profiles of other kinase inhibitors profiled on the same panel. Furthermore, we evaluated



Kinase binding experiments and molecular docking of nemtabrutinib. Sensorgrams of nemtabrutinib and reference inhibitor binding in surface plasmon resonance experiments with MEK1 (a) or B-RAF (b). The red and grey lines represent the experimental results and the black lines represent the fits obtained using a 1:1 binding model. (c) Binding mode of nemtabrutinib in the ATP-binding pocket of BTK (PDB ID: 6E4F). (d) Highest-scoring docking pose of nemtabrutinib in the ATP-binding pocket of MEK1 (PDB ID: 7XLP).

the correlation of the $\rm IC_{50}$ values with gene expression levels, protein expression levels and CRISPR or RNAi gene dependency scores. The inhibitory activity of nemtabrutinib on the identified candidate kinase targets was investigated in biochemical assays and binding to selected targets was evaluated with surface plasmon resonance and molecular docking studies.

In our study, nemtabrutinib showed moderate cellular activity on the BTK-dependent SU-DHL-6 and REC-1 cell lines. Nemtabrutinib was approximately 40- to 200-fold (SU-DHL-6) or 50- to 4000-fold (REC-1) less potent in cell viability assays with these cell lines than approved BTK inhibitors (Supplementary Table S5). It should be noted that BTK inhibitors exert their therapeutic activity by promoting egress of malignant B-cells from lymph nodes (40, 41). Inhibition of tumor cell proliferation is not thought to significantly contribute to their clinical efficacy. Cell viability assays are thus, at best, only a surrogate readout for the activity of BTK inhibitors in B-cell cancers. However, viability assays can be used to identify other therapeutic indications in solid tumors.

Out of the 160 profiled cell lines, nemtabrutinib most potently inhibited the viability of a chronic eosinophilic leukemia cell line (EoL-1), which expresses a chimeric kinase of FIP1L1 and PDGFRα (37) and is, according to the DepMap database (7), strongly dependent on SIK3. While the cellular IC50 profile of nemtabrutinib correlates with CRISPR dependency of SIK3, nemtabrutinib does not bind SIK3 in a biochemical kinase assay. Most likely, the correlation between SIK3 knock-down dependency and the cell panel profiling results is dominated by the potent inhibitory activity on the EoL-1 cell line (Supplementary Figure S3A). In contrast, high FGFR3 gene expression correlated with sensitivity to nemtabrutinib across the whole cell line panel (Supplementary Figure S3B). Cross-reactivity of nemtabrutinib with other growth factor RTKs has been described previously, i.e., with neurotrophic tyrosine receptor kinases (NTRK) (42) and fmsrelated tyrosine kinase 3 (FLT3) (43). Elgamal et al. explored inhibition of FLT3 by nemtabrutinib as a potential treatment option of acute myeloid leukemia (AML) in preclinical models.

In the first article describing nemtabrutinib, therein referred to as ARQ 531, Reiff et al. reported a number of cross-reactivities with other protein kinases besides BTK. Profiling was performed at an ATP concentration of 1 mmol/L ATP, thus mimicking intracellular ATP levels (44). An IC50 of 599 nmol/L was determined in an enzyme assay for MEK1. We used the same protein and assay readout (both from Carna) but performed the assay at $K_{M,bin}$, i.e., an ATP concentration close to $K_{M,ATP}$, which for MEK1 and MEK2 corresponded to 10 µmol/L ATP. Although the cellular ATP concentration is generally between 1-5 mmol/L, using the $K_{M,ATP}$ in biochemical assays allows the IC50 value to become a direct measure of the binding affinity between the investigated compound and the kinase (45). We determined an IC_{50} of approximately 9 nmol/L for MEK1 and MEK2, which is six times higher than its IC₅₀ in the enzyme assay on BTK (Table 1). Reiff et al. reported that nemtabrutinib inhibited MEK1 with a 1200 times higher IC50 than BTK. The cross-reactivity of nemtabrutinib with MEK1 and MEK2 corresponds with the preferential targeting of BRAF-mutant cell lines. Of note, we independently confirmed the higher IC50 on MEK1 in the biochemical enzyme assay at 1 mmol/L ATP (*i.e.*, 456 nmol/L; Table 1).

As mentioned before, X-ray crystallographic studies of nemtabrutinib with BTK indicate that nemtabrutinib is an ATPcompetitive (Type I) inhibitor (15). Our docking studies indicate that it binds in a similar way to MEK1. In contrast, currently approved MEK inhibitors, such as trametinib and cobimetinib, target MEK through an allosteric pocket adjacent to the ATP-binding pocket (Type III inhibitors) (46). Allosteric MEK1 inhibitors are used in combination with B-RAF inhibitors for treating BRAF V600-mutant cancers or as monotherapies for neurofibromatosis type I (47). However, resistance to allosteric MEK inhibitors is frequently observed and can arise through multiple mechanisms. First, mutations in MEK1 or MEK2 can confer cross-resistance to multiple inhibitors within this class. Notably, many of these resistance mutations remain susceptible to ATP-competitive, Type I MEK inhibitors (48, 49). Second, allosteric MEK inhibitors exhibit reduced binding affinity for phosphorylated MEK, which can be caused by overexpression of BRAF (35, 50). In contrast, ATPcompetitive inhibitors retain their affinity against phosphorylated MEK, underscoring another advantage of this binding mode (35).

In addition to the ATP-competitive binding mode of nemtabrutinib, its multi-kinase inhibition profile may provide therapeutic benefits beyond those of selective MEK inhibitors. Reactivation of the MAPK pathway, commonly driven by diminished ERK-mediated negative feedback on RTKs or acquired RTK overexpression, is a prevalent resistance mechanism (51, 52). Our findings indicate that nemtabrutinib not only targets MEK but also inhibits multiple RTKs. This dual mechanism of action can potentially delay MAPK pathway reactivation and extend the duration of response compared to more selective allosteric or ATP-competitive MEK inhibitors.

Taken together, our results show that nemtabrutinib downregulates MAPK signaling by inhibiting MEK1 and that it is also an inhibitor of several growth factor RTKs, including FGFR2, FGFR3 and PDGFR α . The ATP-competitive binding mode of nemtabrutinib in MEK and its dual mechanism of action are promising features that warrant further investigation in MAPK-driven cancers. Our data illustrate the power of combining cell panel profiling, bioinformatics and kinase biochemical profiling for the identification of differentiators and new potential therapeutic applications of kinase inhibitors.

Data availability statement

The original contributions presented in the study are included in the article/Supplementary Material. Further inquiries can be directed to the corresponding author.

Ethics statement

Ethical approval was not required for the studies on cell lines in accordance with the local legislation and institutional requirements because only commercially available established cell lines were used.

Author contributions

DK: Methodology, Investigation, Writing – review & editing, Formal analysis, Visualization. JM: Investigation, Formal analysis, Writing – review & editing. EB: Writing – review & editing, Investigation. JY: Writing – review & editing, Investigation, Formal analysis. JR: Writing – review & editing, Investigation, Methodology, Formal analysis, Writing – review & editing, Methodology, Visualization, Investigation. YG: Visualization, Methodology, Formal analysis, Investigation, Writing – review & editing. JK: Writing – review & editing, Investigation, Formal analysis, Methodology, Supervision. GZ: Resources, Conceptualization, Writing – review & editing, Investigation, Writing – original draft, Formal analysis, Funding acquisition, Supervision.

Funding

The author(s) declare that no financial support was received for the research and/or publication of this article.

Acknowledgments

We would like to thank Prof. Dr. Iwan de Esch (Vrije Universiteit Amsterdam) for helpful discussion on the computational modeling of nemtabrutinib.

Conflict of interest

Authors DK, JM, EB, JY, JR, YG, JK, and GZ were employed by the company Oncolines B.V. The remaining authors declare that the research was conducted in the absence of any commercial or financial relationships that could be construed as a potential conflict of interest.

Generative AI statement

The author(s) declare that no Generative AI was used in the creation of this manuscript.

Any alternative text (alt text) provided alongside figures in this article has been generated by Frontiers with the support of artificial intelligence and reasonable efforts have been made to ensure accuracy, including review by the authors wherever possible. If you identify any issues, please contact us.

Publisher's note

All claims expressed in this article are solely those of the authors and do not necessarily represent those of their affiliated organizations, or those of the publisher, the editors and the reviewers. Any product that may be evaluated in this article, or claim that may be made by its manufacturer, is not guaranteed or endorsed by the publisher.

Supplementary material

The Supplementary Material for this article can be found online at: https://www.frontiersin.org/articles/10.3389/fonc.2025.1667291/full#supplementary-material

References

- 1. Shoemaker RH. The NCI60 human tumour cell line anticancer drug screen. Nat Rev Cancer. (2006) 6:813–23. doi: 10.1038/nrc1951
- 2. Barretina J, Caponigro G, Stransky N, Venkatesan K, Margolin AA, Kim S, et al. The Cancer Cell Line Encyclopedia enables predictive modelling of anticancer drug sensitivity. *Nature*. (2012) 483:603–7. doi: 10.1038/nature11003
- 3. Garnett MJ, Edelman EJ, Heidorn SJ, Greenman CD, Dastur A, Lau KW, et al. Systematic identification of genomic markers of drug sensitivity in cancer cells. *Nature*. (2012) 483:570–5. doi: 10.1038/nature11005
- 4. Uitdehaag JCM, De Roos JADM, Van Doornmalen AM, Prinsen MBW, De Man J, Tanizawa Y, et al. Comparison of the cancer gene targeting and biochemical selectivities of all targeted kinase inhibitors approved for clinical use. *PLoS One.* (2014) 9(3):e92146. doi: 10.1371/journal.pone.0092146
- 5. Uitdehaag JCM, Kooijman JJ, de Roos JADM, Prinsen MBW, Dylus J, Willemsen-Seegers N, et al. Combined cellular and biochemical profiling to identify predictive drug response biomarkers for kinase inhibitors approved for clinical use between 2013 and 2017. *Mol Cancer Ther.* (2019) 18:470–81. doi: 10.1158/1535-7163.MCT-18-0877
- 6. Kooijman JJ, van Riel WE, Dylus J, Prinsen MBW, Grobben Y, de Bitter TJJ, et al. Comparative kinase and cancer cell panel profiling of kinase inhibitors approved for clinical use from 2018 to 2020. *Front Oncol.* (2022) 12. doi: 10.3389/fonc.2022.953013
- 7. Ghandi M, Huang FW, Jané-Valbuena J, Kryukov GV, Lo CC, McDonald ER, et al. Next-generation characterization of the cancer cell line encyclopedia. *Nature*. (2019) 569:503–8. doi: 10.1038/s41586-019-1186-3
- 8. Uitdehaag JCM, De Roos JADM, Prinsen MBW, Willemsen-Seegers N, De Vetter JRF, Dylus J, et al. Cell panel profiling reveals conserved therapeutic clusters and

- differentiates the mechanism of action of different pi3k/mtor, aurora kinase and EZH2 inhibitors. $Mol\ Cancer\ Ther.\ (2016)\ 15:3097-109.\ doi: 10.1158/1535-7163.MCT-16-0403$
- 9. Willemsen-Seegers N, Uitdehaag JCM, Prinsen MBW, de Vetter JRF, de Man J, Sawa M, et al. Compound selectivity and target residence time of kinase inhibitors studied with surface plasmon resonance. *J Mol Biol.* (2017) 429:574–86. doi: 10.1016/j.jmb.2016.12.019
- 10. Barf T, Covey T, Izumi R, Van De Kar B, Gulrajani M, Van Lith B, et al. Acalabrutinib (ACP-196): A covalent Bruton tyrosine kinase inhibitor with a differentiated selectivity and *in vivo* potency profile. *J Pharmacol Exp Ther.* (2017) 363:240–52. doi: 10.1124/jpet.117.242909
- 11. Furman RR, Cheng S, Lu P, Setty M, Perez AR, Guo A, et al. Ibrutinib resistance in chronic lymphocytic leukemia. N Engl J Med. (2014) 370:2352–4. doi: 10.1056/NEJMc1402716
- 12. Woyach JA, Furman RR, Liu TM, Ozer HG, Zapatka M, Ruppert AS, et al. Resistance mechanisms for the bruton's tyrosine kinase inhibitor ibrutinib. *N Engl J Med.* (2014) 370:2286–94. doi: 10.1056/NEJMoa1400029
- 13. Woyach JA, Ruppert AS, Guinn D, Lehman A, Blachly JS, Lozanski A, et al. BTKC4818-Mediated resistance to ibrutinib in chronic lymphocytic leukemia. *J Clin Oncol.* (2017) 35:1437–43. doi: 10.1200/JCO.2016.70.2282
- 14. Mato AR, Woyach JA, Brown JR, Ghia P, Patel K, Eyre TA, et al. Pirtobrutinib after a covalent BTK inhibitor in chronic lymphocytic leukemia. *New Engl J Med.* (2023) 389:33–44. doi: 10.1056/NEJMoa2300696
- 15. Reiff SD, Mantel R, Smith LL, Greene JT, Muhowski EM, Fabian CA, et al. The btk inhibitor arq 531 targets ibrutinib-resistant cll and richter transformation. *Cancer Discov.* (2018) 8:1300–15. doi: 10.1158/2159-8290.CD-17-1409

- 16. Eyre TA, Riches JC. The evolution of therapies targeting Bruton Tyrosine Kinase for the treatment of chronic lymphocytic leukemia: Future perspectives. *Cancers (Basel)* (2023) 15(9):2596. doi: 10.3390/cancers15092596
- 17. Kitagawa D, Yokota K, Gouda M, Narumi Y, Ohmoto H, Nishiwaki E, et al. Activity-based kinase profiling of approved tyrosine kinase inhibitors. *Genes to Cells*. (2013) 18:110–22. doi: 10.1111/gtc.12022
- 18. Metz KS, Deoudes EM, Berginski ME, Jimenez-Ruiz I, Aksoy BA, Hammerbacher J, et al. Coral: clear and customizable visualization of human kinome data. *Cell Syst.* (2018) 7:347–350.e1. doi: 10.1016/j.cels.2018.07.001
- 19. Libouban MAA, De Roos JADM, Uitdehaag JCM, Willemsen-Seegers N, Mainardi S, Dylus J, et al. Stable aneuploid tumors cells are more sensitive to TTK inhibition than chromosomally unstable cell lines. *Oncotarget*. (2017) 8:38309–25. doi: 10.18632/oncotarget.16213
- 20. Conlon NT, Kooijman JJ, van Gerwen SJC, Mulder WR, Zaman GJR, Diala I, et al. Comparative analysis of drug response and gene profiling of HER2-targeted tyrosine kinase inhibitors. *Br J Cancer.* (2021) 124:1249–59. doi: 10.1038/s41416-020-01257-x
- 21. Tate JG, Bamford S, Jubb HC, Sondka Z, Beare DM, Bindal N, et al. COSMIC: the catalogue of somatic mutations in cancer. *Nucleic Acids Res.* (2019) 47:D941–7. doi: 10.1093/nar/gky1015
- 22. Chang MT, Bhattarai TS, Schram AM, Bielski CM, Donoghue MTA, Jonsson P, et al. Accelerating discovery of functional mutant alleles in cancer. *Cancer Discov.* (2018) 8:174–83. doi: 10.1158/2159-8290.CD-17-0321
- 23. Suehnholz SP, Nissan MH, Zhang H, Kundra R, Nandakumar S, Lu C, et al. Quantifying the expanding landscape of clinical actionability for patients with cancer. *Cancer Discov.* (2024) 14:49–65. doi: 10.1158/2159-8290.CD-23-0467
- 24. Chakravarty D, Jianjiong G. OncoKB: A Precision Oncology Knowledge Base (2017). Available online at: http://oncokb.org (Accessed May 29, 2025).
- 25. Meyers RM, Bryan JG, McFarland JM, Weir BA, Sizemore AE, Xu H, et al. Computational correction of copy number effect improves specificity of CRISPR-Cas9 essentiality screens in cancer cells. *Nat Genet.* (2017) 49:1779–84. doi: 10.1038/ng.3984
- 26. Dempster JM, Rossen J, Kazachkova M, Pan J, Kugener G, Root DE, et al. Extracting biological insights from the project achilles genome-scale CRISPR screens in cancer cell lines(2019). Available online at: http://biorxiv.org/lookup/doi/10.1101/720243 (Accessed May 29, 2025).
- 27. Dempster JM, Boyle I, Vazquez F, Root DE, Boehm JS, Hahn WC, et al. Chronos: a cell population dynamics model of CRISPR experiments that improves inference of gene fitness effects. *Genome Biol.* (2021) 22:343. doi: 10.1186/s13059-021-02540-7
- 28. Pacini C, Dempster JM, Boyle I, Gonçalves E, Najgebauer H, Karakoc E, et al. Integrated cross-study datasets of genetic dependencies in cancer. *Nat Commun.* (2021) 12:1661. doi: 10.1038/s41467-021-21898-7
- 29. McFarland JM, Ho ZV, Kugener G, Dempster JM, Montgomery PG, Bryan JG, et al. Improved estimation of cancer dependencies from large-scale RNAi screens using model-based normalization and data integration. *Nat Commun.* (2018) 9:4610. doi: 10.1038/s41467-018-06916-5
- 30. R Core Team. R: A Language and Environment for Statistical Computing (2023). Vienna, Austria: R foundation for Statistical Computing. Available online at: https://www.R-project.org/ (Accessed May 29, 2025).
- 31. Sinkala M. Mutational landscape of cancer-driver genes across human cancers. Sci Rep. (2023) 13:12742. doi: 10.1038/s41598-023-39608-2
- 32. Csardi G, Nepusz T. The igraph software package for complex network research. *Interjournal.* (2006), 1695. Available online at: http://igraph.org.
- 33. Lawrence MS, Stojanov P, Mermel CH, Robinson JT, Garraway LA, Golub TR, et al. Discovery and saturation analysis of cancer genes across 21 tumour types. *Nature*. (2014) 505:495–501. doi: 10.1038/nature12912
- 34. Manning G, Whyte DB, Martinez R, Hunter T, Sudarsanam S. The protein kinase complement of the human genome. *Science* (1979). (2002) 298:1912–34. doi: 10.1126/science.1075762

- 35. Takano K, Munehira Y, Hatanaka M, Murakami R, Shibata Y, Shida T, et al. Discovery of a novel ATP-competitive MEK inhibitor DS03090629 that overcomes resistance conferred by BRAF overexpression in BRAF-mutated melanoma. *Mol Cancer Ther.* (2023) 22:317–32. doi: 10.1158/1535-7163.MCT-22-0306
- 36. Rice KD, Aay N, Anand NK, Blazey CM, Bowles OJ, Bussenius J, et al. Novel carboxamide-based allosteric MEK inhibitors: discovery and optimization efforts toward XL518 (GDC-0973). ACS Med Chem Lett. (2012) 3:416–21. doi: 10.1021/ml300049d
- 37. Cools J, Quentmeier H, Huntly BJP, Marynen P, Griffin JD, Drexler HG, et al. The EOL-1 cell line as an *in vitro* model for the study of FIP1L1-PDGFRA-positive chronic eosinophilic leukemia. *Blood.* (2004) 103:2802–5. doi: 10.1182/blood-2003-07-2479
- 38. Munshi M, Liu X, Chen JG, Xu L, Tsakmaklis N, Demos MG, et al. SYK is activated by mutated MYD88 and drives pro-survival signaling in MYD88 driven B-cell lymphomas. *Blood Cancer J.* (2020) 10:12. doi: 10.1038/s41408-020-0277-6
- 39. Rahal R, Frick M, Romero R, Korn JM, Kridel R, Chun Chan F, et al. Pharmacological and genomic profiling identifies NF-κB-targeted treatment strategies for mantle cell lymphoma. *Nat Med.* (2014) 20:87–92. doi: 10.1038/ms.2435
- 40. de Rooij MFM, Kuil A, Geest CR, Eldering E, Chang BY, Buggy JJ, et al. The clinically active BTK inhibitor PCI-32765 targets B-cell receptor— and chemokine-controlled adhesion and migration in chronic lymphocytic leukemia. *Blood.* (2012) 119:2590–4. doi: 10.1182/blood-2011-11-390989
- 41. Ponader S, Chen SS, Buggy JJ, Balakrishnan K, Gandhi V, Wierda WG, et al. The Bruton tyrosine kinase inhibitor PCI-32765 thwarts chronic lymphocytic leukemia cell survival and tissue homing *in vitro* and *in vivo*. *Blood*. (2012) 119:1182–9. doi: 10.1182/blood-2011-10-386417
- 42. Yu Y, Schwartz G, Schamber P, Savage RE, Eathiraj S, Hall T, et al. Abstract 4797: *In vitro* and *in vivo* effect of ARQ 531 on Trk family kinases. *Cancer Res.* (2018) 78:4797–7. doi: 10.1158/1538-7445.AM2018-4797
- 43. Elgamal OA, Mehmood A, Jeon JY, Carmichael B, Lehman A, Orwick SJ, et al. Preclinical efficacy for a novel tyrosine kinase inhibitor, ArQule 531 against acute myeloid leukemia. *J Hematol Oncol.* (2020) 13:8. doi: 10.1186/s13045-019-0821-7
- 44. Gribble FM, Loussouarn G, Tucker SJ, Zhao C, Nichols CG, Ashcroft FM. A novel method for measurement of submembrane ATP concentration. *J Biol Chem.* (2000) 275:30046–9. doi: 10.1074/jbc.M001010200
- 45. Smyth LA, Collins I. Measuring and interpreting the selectivity of protein kinase inhibitors. *J Chem Biol.* (2009) 2:131–51. doi: 10.1007/s12154-009-0023-9
- 46. Zhao Z, Xie L, Bourne PE. Insights into the binding mode of MEK type-III inhibitors. A step towards discovering and designing allosteric kinase inhibitors across the human kinome. *PLoS One.* (2017) 12:e0179936. doi: 10.1317/journal.pone.0179936
- 47. Cheng Y, Tian H. Current development status of MEK inhibitors. Molecules. (2017) 22:1551. doi: 10.3390/molecules22101551
- 48. Gao Y, Chang MT, McKay D, Na N, Zhou B, Yaeger R, et al. Allele-specific mechanisms of activation of MEK1 mutants determine their properties. *Cancer Discov.* (2018) 8:648–61. doi: 10.1158/2159-8290.CD-17-1452
- 49. Gao Y, Maria A, Na N, da Cruz Paula A, Gorelick AN, Hechtman JF, et al. V211D mutation in MEK1 causes resistance to MEK inhibitors in colon cancer. *Cancer Discov.* (2019) 9:1182–91. doi: 10.1158/2159-8290.CD-19-0356
- 50. Sheth PR, Liu Y, Hesson T, Zhao J, Vilenchik L, Liu YH, et al. Fully activated MEK1 exhibits compromised affinity for binding of allosteric inhibitors U0126 and PD0325901. *Biochemistry*. (2011) 50:7964–76. doi: 10.1021/bi200542r
- 51. Sun C, Wang L, Huang S, Heynen GJJE, Prahallad A, Robert C, et al. Reversible and adaptive resistance to BRAF(V600E) inhibition in melanoma. *Nature.* (2014) 508:118–22. doi: 10.1038/nature13121
- 52. Lake D, Corrêa SAL, Müller J. Negative feedback regulation of the ERK1/2 MAPK pathway. *Cell Mol Life Sci.* (2016) 73:4397–413. doi: 10.1007/s00018-016-2297-8